ARTICLE

Novel Approach for the Assembly of Highly Efficient SERS Substrates

Aline Cerf,*,†,‡ Gábor Molnár,‡,§ and Christophe Vieu†,‡

CNRS, LAAS, 7, avenue du Colonel Roche, F-31077 Toulouse, France, Université de Toulouse, UPS, INSA, INP, ISAE, LAAS, LCC, F-31077 Toulouse, France, and Laboratoire de Chimie de Coordination, CNRS UPR-8241, 205 Route de Narbonne, 31077 Toulouse, France

ABSTRACT In this paper we present the properties of surface-enhanced Raman scattering (SERS) active substrates elaborated by a low-cost approach. Our methodology relying on capillary assembly and soft lithography allows us to generate periodic two-dimensional (2D) matrixes of 100 nm gold nanoparticle patterns in a very precise, cost-efficient, and large-scale manner. For this study, we assembled nanoparticle aggregates of different sizes (one to six particles) in order to determine the influence of the aggregation on the local electric field enhancement. We further demonstrate that this substrate is greatly efficient not only for SERS but also in metal-enhanced fluorescence (MEF) for local enhancement of conventional fluorescence.

KEYWORDS: gold nanoparticles • convective and capillary assembly • soft lithography • SERS • MEF

INTRODUCTION

The miniaturization of objects and their manipulation are the current trends for a great number of applications. In this context, methods to locate and study these systems, sometimes reduced to a single molecule, are required. Optical techniques are very interesting because of their noninvasive, nondestructive, and noncontact nature, but they are in general not sensitive enough to study a single nano-object or isolated molecule. A way to enhance the signal is to position the objects of interest in the close vicinity of noble metal nanocrystals (silver, gold). Such nanocrystals offer remarkable properties due to the localized surface plasmon resonances (SPR) that induce, under the effect of an optical excitation with a frequency close to the SPR, a very intense local electric field enhancement near the surface. This phenomenon has been used for various applications ranging from optical detection of molecules, assisted photochemistry, to applications in the fields of spintronics and chemical sensing. When it comes to optical detection of molecules, the information collected by Raman scattering is richer than that of luminescence. Moreover, there is no need to functionalize the molecule with a fluorophore in the common case where the molecule of interest is not naturally luminescent. The interest in the SERS effect is that the Raman signal enhancement can reach 10^{14}, sufficient to detect a single molecule (1). This technique is now widespread in chemistry, but its use remains more or less empirical and its interpretation controversial. The electromagnetic contribution to the enhancement (a chemical contribution is not excluded) is directly linked to the existence of "hot spots" where the electromagnetic field is locally concentrated. The conception of nanometer-sized structures that allow controlling the position of these hot spots is the heart of intense research, both theoretical and experimental (2, 3). What is known, however, is that some of these properties only appear with very precise arrangements, such as regularly spaced coupled particles with short interparticle distance, for instance (4, 5). Nanosphere lithography (6−9) is currently one of the most reproducible and large-scale techniques used to generate substrates with controlled hot spots (10). However, to generate them, several sometimes expensive technological steps are required. Alternatively, a template-assisted colloidal assembly has been employed to create colloidal patterns. For instance, Hyun et al. have used the reversible nature of buckling to fabricate lines of colloids on a flat surface (11). This method can handle any type of colloidal particle but has not proved its efficiency in creating arrays with single-particle resolution. Maury et al. have patterned self-assembled monolayers by nanoimprint lithography, but the patterns obtained with this technique are still difficult to control (12). Xia et al. have combined the dewetting of colloidal dispersions from a structured photoresist substrate with capillary force and geometric confinement to assemble colloids into arrangements with well-defined sizes, shapes, and structures. Nevertheless, if we want to build up more complex scaffolds from these templates, the resist needs to be removed with ethanol or hydrogen plasma and this additional processing is not always possible, depending on the object and the application sought (13). Yan et al. have generated nice and very well-defined nanoparticle cluster arrays, but here again their process requires heavy steps such as e-beam patterning and lift-off (14).

Capillary force assembly (CFA) has already shown its potentiality to create Au nanoparticle assemblies with single-particle resolution (15−17). In the present paper, we dem-

* To whom correspondence should be addressed. Tel: +33-561-33-78-39. Fax: +33-561-33-92-08. E-mail: acerf@laas.fr.

Received for review July 17, 2009 and accepted October 22, 2009

† CNRS, LAAS.

‡ Université de Toulouse.

§ Laboratoire de Chimie de Coordination, CNRS UPR-8241.

DOI: 10.1021/am900476d

Published on Web 10/29/2009

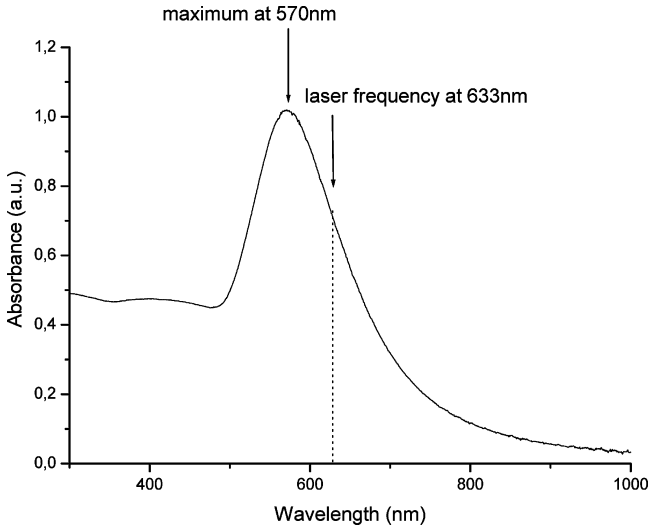

FIGURE 1. Absorbance spectrum of the as-received gold colloid suspension.

onstrate how the combination of capillary assembly with soft lithography can be used as a much more straightforward and affordable procedure to generate in a controlled and regular manner those electromagnetic hot spots with high coverage rate (ideally 10^8 hot spots per square centimeter). Recently, we have shown that, through this methodology, we are able to precisely position gold nanoparticles along a periodic 2D matrix (18). In the present paper, we aim at proving the efficiency of such an arrangement as a SERS substrate. The arrangement and the number of nanoparticles giving the highest increase of the Raman intensity will be discussed.

EXPERIMENTAL SECTION

Gold Colloid Preparation. Citrate-stabilized gold particles with a nominal size of 100 nm in diameter were purchased from Eloïse SARL (5.6×10^9 particles/mL in H_2O). The gold particles were reconcentrated three times and put in suspension into 1 wt % Triton X-100 solution (purchased from VWR International) in deionized water. We voluntarily chose to keep the gold nanoparticles negatively charged by the citrate ligands so that the interparticle distance is fixed and kept constant by those ligands. An absorbance measurement was performed on the commercial gold nanoparticle suspension using a Cary50 spectrophotometer (Figure 1). A broad SPR band was found around 570 nm.

Preparation of Nanostructured Optically Active Substrates. Elastomeric stamp fabrication for microcontact printing (μCP) has been described previously (19). Here we use stamps fabricated from polydimethylsiloxane (PDMS; Sylgard 184 Kit Dow Corning) that are replicated from a silicon-based master structured by electron beam lithography. In the present study, the silicon master used to generate the corresponding PDMS stamp consists of eight $100 \times 100\ \mu m^2$ matrixes with square-shaped patterns of 200, 250, 300, and 370 nm in side, with a period of 3 and 1.5 μm for each of the pattern sizes mentioned. The nominal depth of the structures was set to 120 nm. The stamps were cut in 1 cm $\times$ 1 cm pieces. We voluntarily chose larger structures with respect to the size of the gold nanoparticles in order to have a sampling of different numbers of particles in each pattern for the study of SERS effect dependency on the number of particles.

The technique of directed capillary assembly that we use offers the possibility to direct the assembly of objects: in other words, to single out a chosen number of particles from a complex solution and to precisely position them onto a surface (17, 20). This high-precision inking is carried out using a dedicated setup. It is based on the confinement of particles induced at the three-phase contact line of a droplet that is dragged over a substrate. The nanostructured PDMS stamp on which we want the gold nanoparticles to be assembled is placed on a motorized translation stage below a fixed glass slide at a distance of about 1 mm. A 30 μL droplet of gold nanoparticles in suspension is injected between the glass and the substrate. The liquid meniscus is then moved over the substrate at a velocity of 1 μm/s (Scheme 1). The temperature is set to 27 °C by a Peltier cell which is monitored through a controller, allowing a high accuracy and fast temperature control. The entire setup is equipped with an optical microscope and a CCD camera for direct visualization and recording of the assembly. The experimental parameters (speed, temperature, concentration) are adjusted to enable the assembly of gold nanoparticles with high placement accuracy. The detailed physical mechanisms taking place during directed capillary assembly have already been discussed in previous articles (20).

To transfer the formed gold nanoparticle arrays onto a solid surface, a droplet of solvent (ethanol or deionized water) is placed on the surface (silicon wafer or glass slide) coated by vapor deposition of 3-aminopropyltriethoxysilane (APTES) molecules. The PDMS stamp with the assembled gold nanoparticles is then brought into contact with the APTES-coated surface. This ensemble is placed in an oven at 100 °C for a few minutes to evaporate all the solvent, and the PDMS stamp is then peeled away (Scheme 1) (18).

The obtained gold nanoparticle arrays were characterized by dark field microscopy (×50 objective lens) and scanning electron microscopy (SEM).

Adsorption of Rhodamine 6G, CY5, and Oregon Green Molecules on Nanostructured Optically Active Substrates. For subsequent SERS and MEF experiments, we selected positively charged dye molecules to increase the probability of electrostatically attaching them on the negatively charged particles (21). Thereafter, a droplet of 1×10^{-6} M Rhodamine 6G or Cyanine 5 aqueous solution (purchased from Sigma Aldrich) was deposited on the nanostructured substrates previously described and left to dry in the dark, at room temperature for SERS and MEF measurements, respectively. Regarding MEF, a control experiment was prepared by depositing a 100 nm thick gold layer on the nanostructured substrate with a sputterer (from Varian) before incubation for 1 h in 15 mM cysteamine solution in deionized water. Here, cysteamine molecules ($HSCH_2CH_2NH_2$) bind to the gold layer through their thiol group. Later, after thorough washing with deionized water and drying with flowing nitrogen, this cysteamine-modified substrate was incubated with 0.001 % Oregon green solution (2′,7′-difluorofluorescein from Molecular Probes, Invitrogen) in phosphate saline buffer (PBS) for 4 h in the dark. This step leads to the covalent binding of Oregon green molecules to the free amine groups of the cysteamine molecules. Finally, the substrate was thoroughly washed with PBS and dried under flowing nitrogen.

Raman Characterization. Raman spectra were recorded in the 600−1700 cm^{-1} range using a Jobin Yvon Labram HR800 Raman spectrometer. The spectrometer consists of a BXFM (Olympus) optical microscope, a single-grating spectrograph (600 grooves mm^{-1}, focal length (f) 800 mm) and a thermoelectrically cooled 1024 $\times$ 256 pixels CCD detector (Andor) operating at −70 °C. The entrance slit was kept at 100 μm, and a spectral resolution of ca. 4 cm^{-1} was obtained. The 632.8 nm line of a 3 mW He−Ne laser was used as the excitation source. Plasma lines were removed using a narrow-band interference filter, and the exciting radiation was focused on the sample via a 100× objective (numerical aperture (NA) 0.9). The laser power at the sample was filtered by appropriate neutral density filters

Scheme 1. Schematic Representation of the Procedure for Generating an Optically Active Substrate: (1) Capillary Assembly of 100 nm Gold Particles on a Nanostructured PDMS Stamp; (2) Structured PDMS Stamp with Assembled Gold Nanoparticles; (3) Transfer Printing of These Nanoparticles on an APTES-Coated Silicon Substrate by Solvent Mediation; (4) Peeling Away of the PDMS Stamp

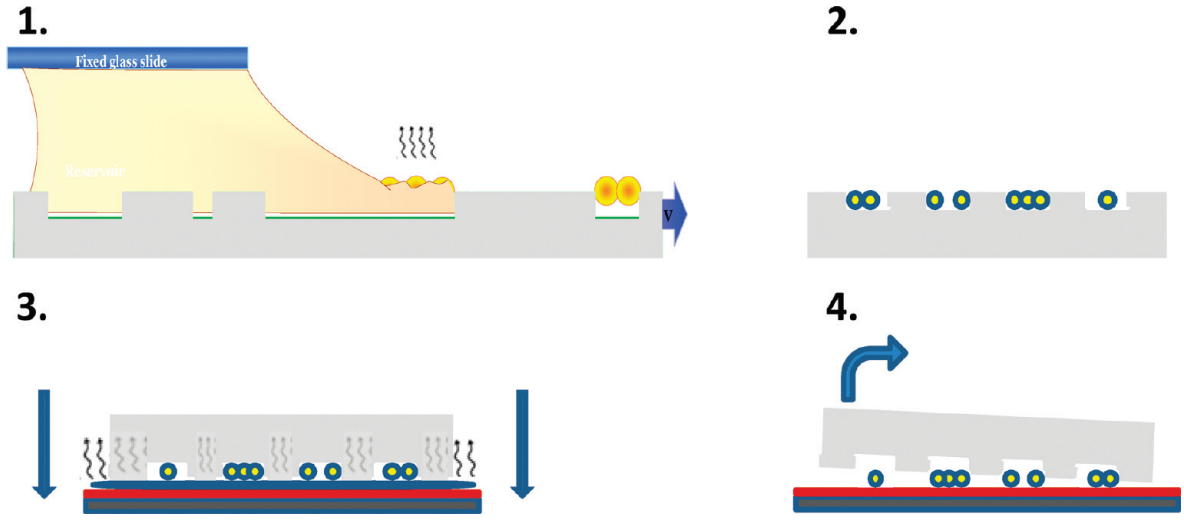

and fixed at 30 μW on a measured spot diameter of ca. 0.5 μm. The scattered light was collected in a backscattering configuration, using the same microscope objective, and the Rayleigh scattering was removed by means of a holographic notch filter. All spectra were calibrated with respect to the silicon Raman mode at 520.7 cm^{-1}. Each measurement was performed under ambient conditions and was accumulated twice with an acquisition time of 1 s. Cartographies were performed on a defined area of the gold nanoparticle matrixes. A half-wave plate was used to change the polarization direction of the incident laser. To analyze the polarization state of scattered photons, a linear polarizer with vertical or horizontal direction of polarization axis has been used. No correction for the spectrograph response was performed, as we use a grating which is fairly insensitive to the polarization changes.

MEF Characterization. Both the substrate with CY5 molecules and the substrate modified with Oregon green molecules were studied using an Olympus BX-51 microscope equipped with an Hg lamp as an excitation light source and two bandpass fluorescence optical filter sets (~480−550/590 and ~460−490/520 nm, respectively). Fluorescence images were acquired with an Andor iXon 897 (512 × 512 pixels) camera. Samples were observed through 60× and 100× objectives.

RESULTS AND DISCUSSION

Figure 2A shows the results obtained after directed assembly of gold nanoparticles on the nanostructured PDMS stamp and transfer printing on APTES-coated silicon with solvent mediation. We can observe from the dark field image that the assembly, which was performed on a large zone of the PDMS stamp (1 cm^2), is transferred on the silicon substrate with very high fidelity in 97% yield (18). No particle remains on the PDMS stamp after printing: all the PDMS pattern cavities of all sizes are empty, and the totality of the particles is transferred. This high transfer rate is observed regardless of the size of the pattern. For the present study we will focus on the 200 and 250 nm side patterns, as in this region we can already obtain an interesting sampling with different numbers of nanoparticles. If we carefully look at the dark field micrograph (Figure 2A), we observe that the assembled particles retain their optical properties. In fact, single particles scatter visible light more efficiently in the blue spectral region and, in contrast, aggregates of nanoparticles tend to scatter more light in the red region. Of course, this difference in light scattering not only depends on the number of particles but also on their shape and particular arrangement. To study more in detail the optical properties of gold nanoparticles depending on their number and arrangement, we used Raman spectroscopy. We measured the Raman signal at regular intervals of an area of the gold nanoparticle matrix. We observe from the resulting Raman cartography (Figure 2B) that, despite the short acquisition time used and the low laser power, we obtained a significant increase of the Raman signal at the specific sites corresponding to the particle patterns. We see that the obtained spectra (Figure 2C) correspond to the Rhodamine 6G reference spectrum previously reported with strong Raman peaks at 1182, 1188, 1312, 1347, 1366, 1511, and 1655 cm^{-1} in particular (22−24). Note that the peak at 1600 cm^{-1} corresponds to organic residues. Camden et al. (25) described a blinking phenomenon occurring in the case of a Rhodamine 6G−citrate−particle system that we observe here again: Figure 2D shows a waterfall plot of Rhodamine 6G spectra collected from a single aggregate over time. At the beginning of the acquisition, the spectrum appears to have only Rhodamine 6G character, but as the time progresses, the spectrum changes around $t = 150$ s and a few seconds later recovers its initial and characteristic profile over the course of 360 s, as displayed in the figure. This phenomenon could explain the variations observed among the spectra here presented (Figures 2D and 3). If we look at the Raman cartography carefully, we further notice that this local enhancement varies among the patterns. To comprehend this phenomenon in particular, we imaged that same area with a scanning electron microscope. The confrontation of several Raman cartographies with their corresponding SEM image revealed that the greatest enhancement is provoked by aggregates of particles, whereas a single

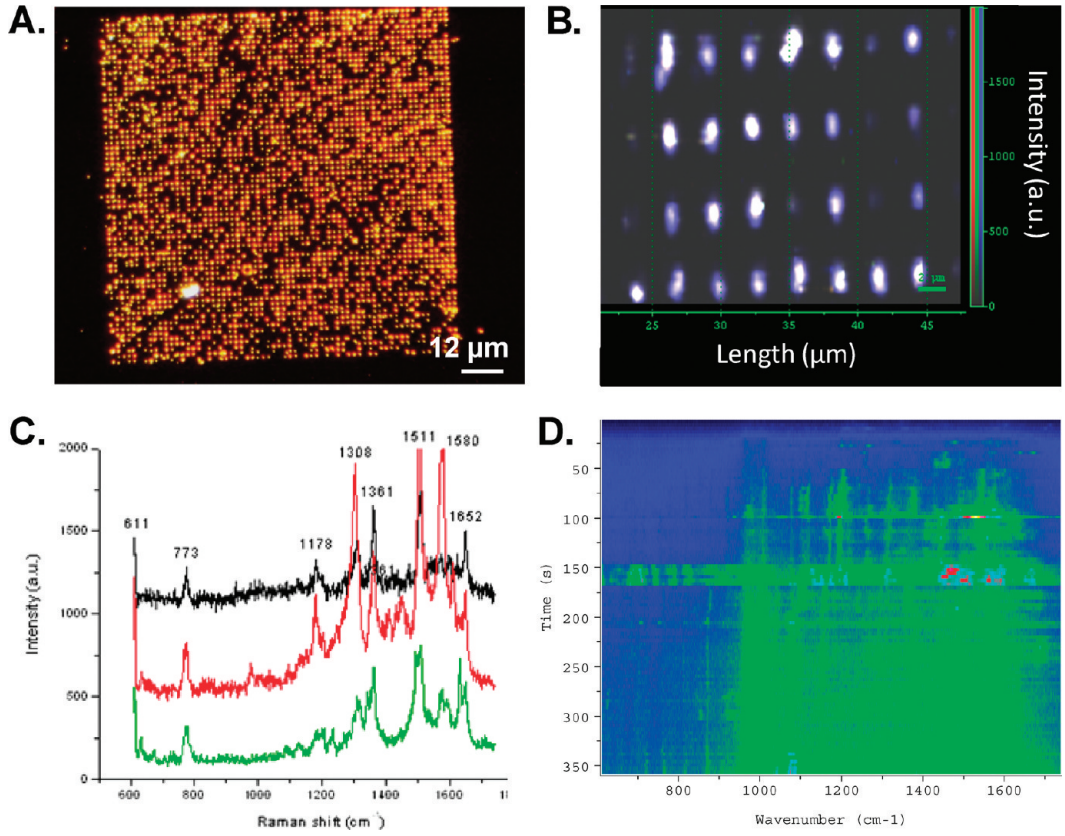

FIGURE 2. (A) Dark field image of a gold nanoparticle periodic matrix on an APTES-coated silicon wafer after transfer (300 nm side patterns with 1.5 μm spacing). (B) Raman cartography (130 $\times$ 130 scans with 0.2 μm step size, recorded at 1312 cm^{-1}) of an area of a gold nanoparticle matrix incubated with Rhodamine 6G (370 nm side patterns with 3 μm spacing). (C) Example of the spectra obtained at different bright spots of the Raman cartography. (D). Time series waterfall plot of Rhodamine 6G Raman spectra collected from a single active aggregate with the false color representing signal intensity, where green to red is highest and blue or black is lowest.

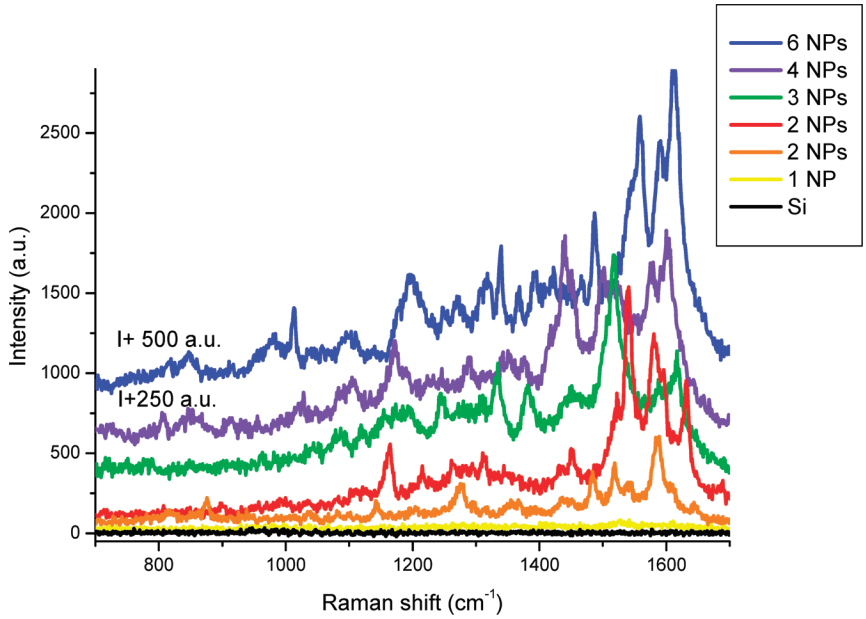

FIGURE 3. Raman spectra of Rhodamine 6G molecules obtained for different numbers of particles. Spectra in red and orange correspond to dimers with different orientations.

nanoparticle provokes only a relatively small enhancement. This remark joins the observations previously reported by Khan et al. (26, 27). The phenomenon could be explained by the fact that the resonance varies depending on the size of the aggregate: the resonance of large aggregates shifts toward the red spectral region (14). Consequently, by using a 633 nm excitation laser, we are closer to the resonance of larger aggregates and thus favor the enhancement of their scattering in comparison with that of small aggregates or single nanoparticles (14). This implies that the observations

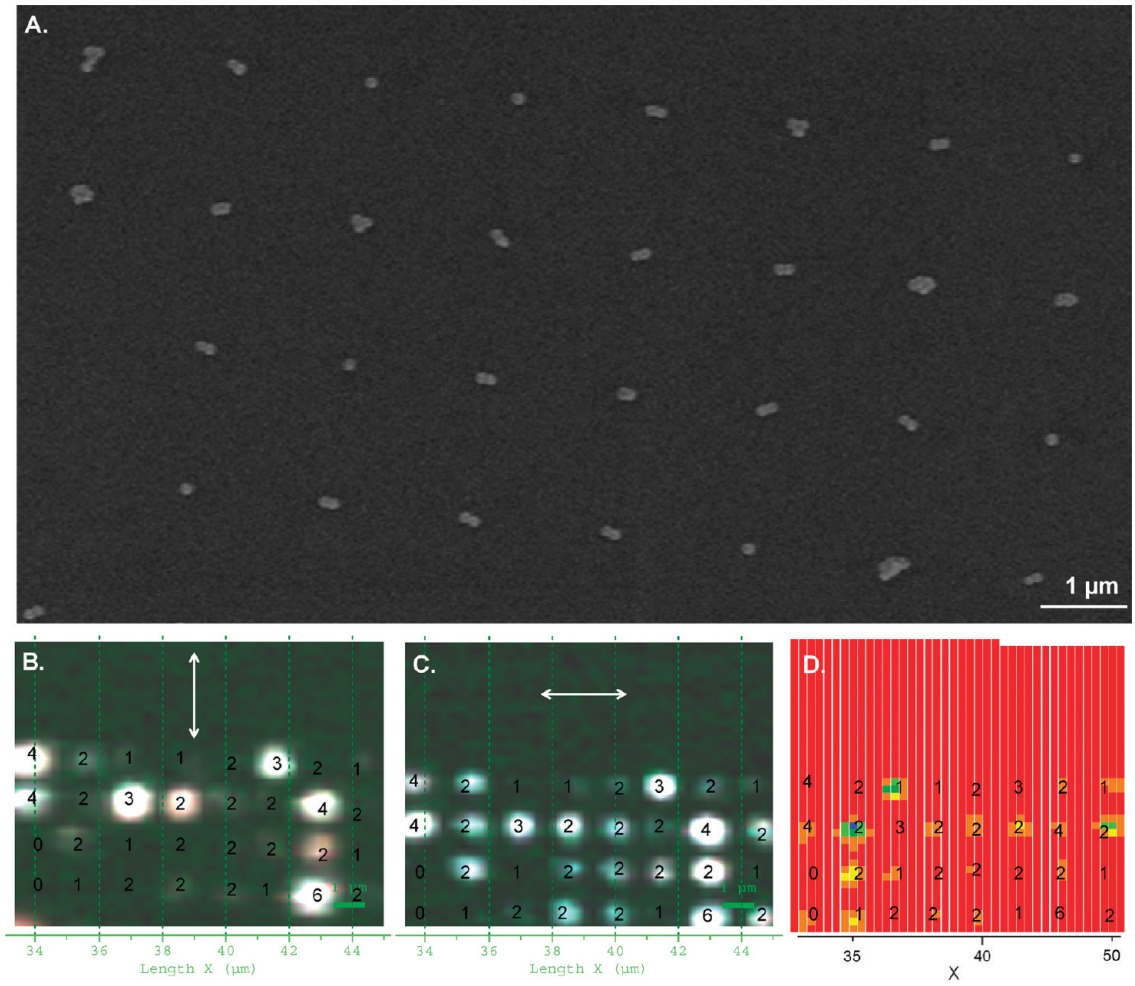

FIGURE 4. Study of the influence of the analyzer orientation. (A) SEM image corresponding to Raman cartographies (B) and (C) (200 nm side patterns with 1.5 μm spacing). Part (B) corresponds to a vertical analyzer, and (C) corresponds to a horizontal analyzer, as shown (40 $\times$ 40 scans with 0.3 μm step size). (D). Cartography corresponding to (C) data subtracted from (B) data with false color representing signal intensity, where orange to green or blue is highest and red is lowest.

here described may have been different with another excitation wavelength. Furthermore, electric-field simulations have shown that hot spots are located between the nanoparticles (4, 28): this could also be an important explanation to the observed differences between single gold particles and agglomerations of several particles. We reported in Figure 3 the Raman spectra recorded at different patterns of the matrix corresponding to a given number of particles. By superposing the spectra, we clearly notice that the spectrum corresponding to one nanoparticle is hardly more intense than that measured on plain silicon. For an arrangement of three nanoparticles, the characteristic peaks of the Rhodamine spectrum are strongly enhanced, but further increases in the number of particles (up to six) do not lead to significantly higher intensities, in agreement with the observations of Yan et al. (14) claiming that no further red shift occurs above three particles. The dimers exhibit also high enhancements, but their SERS efficiency seems more sensitive, depending on their orientation (Figure 3). To confirm this interesting observation, we fixed the incident polarization of the laser, which is vertical, and we added an analyzer that lets the scattered photons only pass through two directions (either vertical or horizontal). We recorded two cartographies, one with a vertical analyzer and one with a horizontal analyzer, and the comparison of these two cartographies clearly reveals an ON/OFF switch behavior (Figure 4). Figure 4D shows the result we obtain by subtracting the cartography recorded with a horizontal analyzer from the cartography recorded with a vertical analyzer. If we further correlate the resulting cartography to the corresponding SEM image, we observe that effectively, by a majority, dimers are sensitive to the analyzer direction. In fact, there exist particular orientations of the dimers with respect to the analyzer that appear to be preferential to obtain the highest enhancement. Conversely, a perpendicular orientation of dimers with respect to the analyzer switches the SERS effect off. Aggregates of three or more nanoparticles do not seem to be influenced so dramatically by the analyzer orientation, as they exhibit less anisotropy. The efficiency of our SERS substrate is difficult to quantify. If we base ourselves on the enhancement factor (EF) calculations found in the literature, these are controversial and nonrealistic in most cases. In the present study it is very difficult to estimate the exact number of molecules covered by the laser spot. However, we can roughly estimate the EF obtained for Rhodamine 6G Raman spectra in the case of an optimal arrangement of three

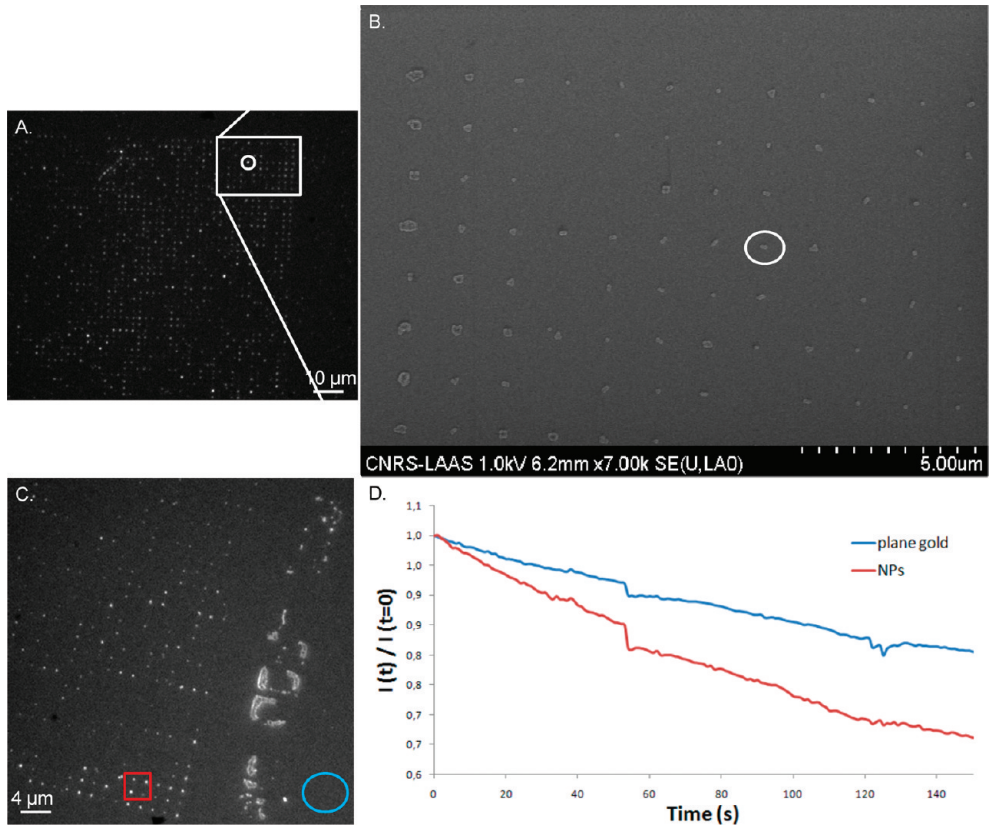

FIGURE 5. MEF effect: (A) fluorescence image of CY5 molecules deposited on a silicon substrate with arrays of gold nanoparticles; (B) enlarged SEM image (the circles mark the corresponding locations in the SEM image in (A); 250 nm side patterns with 1.5 μm spacing); (C) fluorescence image of Oregon green molecules deposited on a silicon substrate with arrays of gold nanoparticles covered with a gold layer; (D) photobleaching measurement performed on two different regions of the substrate, as shown by blue and red marks in (C), with the blue curve corresponding to fluorophores located in the plane gold region and the red curve corresponding to MEF fluorophores located on the gold nanostructures. The curves are normalized with respect to their maxima.

nanoparticles without emitting any assumption on the surface density of molecules adsorbed on the nanoparticles. On the basis of the EF reported for a single 100 nm gold nanoparticle (24) and on the measured Raman intensity ratio between three nanoparticles and one nanoparticle, we estimate that the maximum enhancement factor in our case is 6×10^4. It is worth noticing that this estimation corresponds to the particular case of Rhodamine 6G molecules. What we can affirm is that, with our methodology, hot spots can be generated with a small number of particles, increasing the possibility of detecting small numbers of molecules.

As a further step in this development, we decided to verify whether this highly efficient SERS substrate could also be a good metal-enhanced fluorescence (MEF) substrate (29, 30). For this purpose we selected a fluorophore that can be excited at a wavelength close to that of the gold SPR. We first deposited CY5 fluorophore on our nanostructured optically active substrate. Instead of obtaining a homogeneously red substrate, the fluorescence image obtained revealed that fluorescence is effectively enhanced in the precise sites that correspond to the gold particle patterns (Figure 5). We correlated the fluorescence micrograph to the corresponding SEM image, and we observed that, once again, single nanoparticles do not provoke any significant fluorescence enhancement in comparison to larger aggregates. This result already suggests that there is a local enhancement of plasmonic origin occurring. To further confirm these first observations obtained with a CY5 molecule, we generated another substrate with a different configuration. In this case we chose not to have an electrostatic binding between a positively charged dye and the negatively charged gold nanoparticles. The purpose here is to deposit a layer of gold everywhere onto our substrate with gold nanoparticle arrays and use an intermediate thiol chemistry so that the deposition of the dye is made in a homogeneous manner all over the substrate. In this manner we can simultaneously compare between a nonstructured gold surface and a surface with gold nanoparticle structuration that will have undergone the same functionalization. Thus, we deposited a layer of gold onto one of our optically active substrates with gold nanoparticles. Dark-field and SEM characterizations confirmed that the gold film deposited is continuous: only the larger aggregates can be distinguished, but the smaller aggregates are smeared out. We then deposited an amine-terminated thiol so that the Oregon green dyes subsequently incubated are homogeneously deposited all over the substrate. The resulting fluorescence micrographs reveal that, even with this thick layer of gold, the gold nanoparticle patterns still lead to hot spots that locally amplify the fluorescence signal. To further prove this affirmation, we performed a photobleaching measurement upon prolonged exposure to the incident radiation. The slope of the photobleaching curve in

its initial part revealed that the fluorophore located on the gold nanoparticle patterns photobleaches 2 times faster than the fluorophore located in the outside region of the gold nanoparticle patterns. This result implies that there is an increase in the excitation rate of the fluorophore (more excitation/emission cycles per time unit), suggesting an enhancement mechanism occurring locally. However, there is likely to be an increase of the local temperature as well, and this factor cannot be neglected in the overall interpretation. We are currently working on this particular point to determine the exact contribution of plasmonic or thermodynamic mechanisms to this global phenomenon.

CONCLUSIONS

We have demonstrated that the highly ordered nanostructures we have generated by capillary assembly and soft lithography are efficient SERS substrates. For this study, the optically active substrates consist of periodic 2D matrixes of gold nanoparticles with different nanoparticle arrangements. By means of Raman spectroscopy, we have evidenced that the greatest local electric field enhancement is provoked by aggregates of particles (three to six), whereas a single nanoparticle provokes only a relatively small enhancement. Dimers also exhibit high enhancements, but their SERS efficiency depends on their orientation: a perpendicular orientation of dimers with respect to the analyzer switches the SERS effect off. We further proved the efficiency of this substrate as a MEF substrate for local enhancement of conventional fluorescence. This kind of substrate can easily be fabricated with prefunctionalized metallic particles and could be coupled with other selective and automatized deposition methods (31). One could later imagine evolving toward a label-free biochip with optical readout by coupling, for example, SERS substrates with biological molecules or cells for high-sensitivity monitoring of specific interactions.

Acknowledgment. This work was supported by the EC-funded project NaPa (Contract No. NMP4-CT-2003-500120) and the ANR NANOMOL project. We thank Franck Carcenac and Christian Bergaud from LAAS-CNRS. We also thank Lionel Rechignat and Lionel Salmon from the LCC for their help and Guillaume Charrière from the Pharmacology and Structural Biology Institute (IPBS) for MEF characterization and fruitful discussions.

REFERENCES AND NOTES

(1) Nie, S. M.; Emory, S. R. *Science* **1997**, *275*, 1102–1106.
(2) Käll, M.; Xu, H.; Johansson, P. *J. Raman Spectrosc.* **2005**, *36*, 510–514.
(3) For a recent review see: *Chem. Soc. Rev.* **2008**, *37*.
(4) Haynes, C. L.; McFarland, A. D.; Duyne, R. P. V. *Anal. Chem.* **2005a**, *77*, 338A–346A.
(5) Xu, H.; Aizpurua, J.; Käll, M.; Apell, P. *Phys. Rev. E* **2000**, *62*, 4318–4324.
(6) Hulteen, J. C.; Van Duyne, R. P. *J. Vac. Sci. Technol. A* **1995**, *13*, 1553.
(7) Kosiorek, A.; Kandulski, W.; Glaczynska, H.; Giersig, M. *Small* **2005**, *1*, 439.
(8) Zhang, G.; Wang, D.; Mohwald, H. *Nano Lett.* **2007**, *7*, 127.
(9) Fredriksson, H.; Alaverdyan, Y.; Dmitriev, A.; Langhammer, C.; Sutherland, D. S.; Zach, M.; Kasemo, B. *Adv. Mater.* **2007**, *19*, 4297–4302.
(10) Jensen, T. R.; Duval Malinsky, M.; Haynes, C. L.; Van Duyne, R. P. *J. Phys. Chem. B* **2000**, *104*, 10549–10556.
(11) Hyun, D. C.; Moon, G. D.; Cho, E. C.; Jeong, U. Y. *Adv. Funct. Mater.* **2009**, *19*, 2155–2162.
(12) Maury, P.; Peter, M.; Mahalingam, V.; Reinhoudt, D. N.; Huskens, J. *Adv. Funct. Mater.* **2005**, *15*, 451–457.
(13) Xia, Y. N.; Yin, Y. D.; Lu, Y.; McLellan, J. *Adv. Funct. Mater.* **2003**, *13*, 907–918.
(14) Yan, Bo.; Thubagere, A.; Premasiri, W. R.; Ziegler, L. D.; Dal Negro, L.; Reinhard, B. M. *ACS Nano* **2009**, *3*, 1190–1202.
(15) Rivera, T.; Lecarme, O.; Hartmann, J.; Inglebert, R. L.; Peyrade, D. *Microelec. Eng.* **2009**, *86*, 1089–1092.
(16) Rivera, T.; Lecarme, O.; Hartmann, J.; Rossitto, E.; Berton, K.; Peyrade, D. *J. Vac. Sci. Technol. B* **2008**, *26*, 2513–2519.
(17) Kraus, T.; Malaquin, L.; Schmid, H.; Riess, W.; Spencer, N. D.; Wolf, H. *Nat. Nanotechnol.* **2007**, *2*, 570–576.
(18) Cerf, A.; Vieu, C *Colloids Surf. A* **2009**, *342*, 136–140.
(19) Thibault, C.; Séverac, C.; Trévisiol, E.; Vieu, C. *Microelec. Eng.* **2006**, *83*, 1513–1516.
(20) Malaquin, L.; Kraus, T.; Schmid, H.; Delamarche, E.; Wolf, H. *Langmuir* **2007**, *23*, 11513–11521.
(21) Bell, S. E. J.; Sirimuthu, N. M. S. *Chem. Soc. Rev.* **2008**, *37*, 1012–1024.
(22) Chen, J.; Martensson, T.; Dick, K. A.; Deppert, K.; Xu, H. Q.; Samuelson, L.; Xu, H. *Nanotechnology* **2008**, *19*, 275712.
(23) Saini, G. S. S.; Kaur, S.; Tripathi, S. K.; Mahajan, C. G.; Thanga, H. H.; Verma, A. L. *Spectrochim. Acta, Part A* **2005**, *61*, 653–658.
(24) Wei, H.; Håkanson, U.; Yang, Z.; Höök, F.; Xu, H. *Small* **2008**, *4*, 1296–1300.
(25) Camden, J. P.; Dieringer, J. A.; Zhao, J.; Van Duyne, R. P. *Acc. Chem. Res.* **2008**, *41*, 1653–1661.
(26) Khan, I.; Cunningham, D.; Graham, D.; McComb, D.; Smith, W. E *J. Phys. Chem. B* **2005**, *109*, 3454–3459.
(27) Khan, I.; Cunningham, D.; Littleford, R. E.; Graham, D.; Smith, W. E.; McComb, D. W. *Anal. Chem.* **2006**, *78*, 224–230.
(28) Hao, E.; Schatz, G. C. *J. Phys. Phys.* **2004**, *120*, 357–366.
(29) Yamaguchi, T.; Kaya, T.; Takei, H. *Anal. Biochem.* **2007**, *364*, 171–179.
(30) Shankar, S. S.; Rizzello, L.; Cingolani, R.; Rinaldi, R.; Pompa, P. P. *ACS Nano* **2009**, *3*, 893–900.
(31) Leichle, T.; Saya, D.; Pourciel, J. B.; Mathieu, F.; Nicu, L.; Bergaud, C. *Sens. Actuators A-Phys.* **2006**, *132*, 590–596.

AM900476D